BIOCHEMISTRY
including biophysical chemistry & molecular biology

Article

pubs.acs.org/biochemistry

Structural Alterations of Lamin A Protein in Dilated Cardiomyopathy

Pritha Bhattacharjee, Avinanda Banerjee, Amrita Banerjee, Dipak Dasgupta,* and Kaushik Sengupta*

Biophysics Division, Saha Institute of Nuclear Physics, 1/AF Bidhannagar, Kolkata 700064, India

Supporting Information

ABSTRACT: Lamin A protein, encoded by the *LMNA* gene, belongs to the type V intermediate filament protein family and is a major nuclear protein component of higher metazoan organisms, including humans. Lamin A along with B-type lamins impart structural rigidity to the nucleus by forming a lamina that is closely apposed to the inner nuclear membrane and is also present as a filamentous network in the interior of the nucleus. A vast number of mutations that lead to a diverse array of at least 11 diseases in humans, collectively termed laminopathies, are being gradually uncovered in the *LMNA* gene. Dilated cardiomyopathy (DCM) is one such laminopathy in which ventricular dilation leads to an increase in systolic and diastolic volumes, resulting in cardiac arrhythmia and ultimately myocardial infarction. The point mutations in lamin A protein span the entire length of the protein, with a slight preponderance in the central α-helical coiled-coil forming domain. In this work, we have focused on three such important mutations that had been previously observed in DCM-afflicted patients producing severe symptoms. This is the first report to show that these mutations entail significant alterations in the secondary and tertiary structure of the protein, hence perturbing the intrinsic self-association behavior of lamin A protein. Comparison of the enthalpy changes accompanying the deoligomerization process for the wild type and the mutants suggests a difference in the energetics of their self-association. This is further corroborated by the formation of the aggregates of different size and distribution formed inside the nuclei of transfected cells.

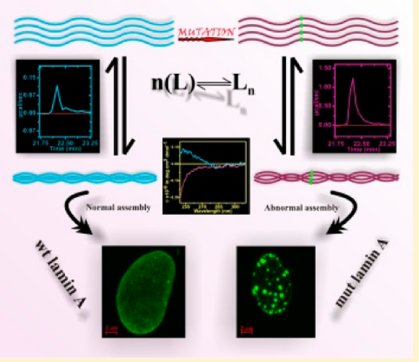

Lamins are type V intermediate filament nuclear proteins imparting structural integrity and rigidity to the nucleus of mostly all metazoan cells but are absent in plants and unicellular organisms.[1,2] Lamins are the principal components of the nuclear lamina apposed between the inner nuclear membrane and the peripheral heterochromatin. These detergent and high-salt resistant proteins are broadly classified into two major categories of types A and B. Most vertebrates with some exceptions express one A-type lamin and two B-type lamins, B1 and B2. In vertebrates, alternative splicing of the *LMNA* gene yields two major isoforms, lamin A and C,[3] whereas lamin AΔ10[4] and lamin C2[5] are reported to be minor isoforms. Lamin B1 and lamins B2 and B3 are encoded by *LMNB1* and *LMNB2*, respectively.[6] A-Type lamin expression appears in tissues only from the onset of differentiation[7,8] in the process of development, whereas at least one B-type lamin is expressed right from embryogenesis. Similarly, human and mouse stem cells express B1 and B2 types but no A type.[9] However, recent reports have shown the presence of lamin A/C in mouse embryonic stem cells.[10] The lamin proteins have a typical structure representative of the intermediate filament protein family consisting of a central α-helical coiled-coil-forming rod domain flanked by a short N-terminal "head" domain and a longer "tail" domain at the carboxy terminus. The rod domain consists of four α-helical heptad repeat-containing subregions demarcated by coils 1A, 1B, 2A, and 2B each separated from the other by flexible linker regions termed L1, L12, and L2.[11] The head and tail domains of the lamins are grossly unstructured, making the protein less favorable for a holistic structural analysis. However, the tail domain contains a stretch of highly conserved residues that make up the Ig fold, the structure of which has been determined by both nuclear magnetic resonance and X-ray crystallography in the case of lamin A.[12,13] The "stutter" region of coil 2B of lamin A has been structurally resolved by X-ray crystallography.[14] Although the mode of stepwise assembly of vertebrate lamins into network like structures inside the cells remains elusive, extensive *in vitro* analysis with bacterially expressed and purified proteins has established that the first step of assembly starts with the formation of coiled-coil left-handed superhelical dimers associated laterally. The next step involves the head-to-tail polarized interaction of the dimers to form tetrameric protofilaments.[15] Four such protofilaments are laterally compacted to form a 10 nm cross-sectional filament.[15−17] Vertebrate lamins continue to assemble further beyond this point at a lowered pH when paracrystalline arrays with regular axial repeat patterns are formed.[15−18] Over the past decade, there has been renewed interest in the study of nuclear lamins, largely because of the fact that nearly 400 mutations have been uncovered in the *LMNA* gene alone, which lead to a plethora of diseases termed laminopathies like autosomal dominant Emery-Dreifuss muscular dystrophy (AD-EDMD),[19] dilated cardiomyopathy (DCM),[20] Hutchinson-Gilford progeria syndrome

Received: March 15, 2013
Revised: May 22, 2013
Published: May 23, 2013

dx.doi.org/10.1021/bi400337t | *Biochemistry* 2013, 52, 4229−4241

(HGPS), atypical Werner's syndrome (WS), restricted dermopathy (RD), and mandibuloacral dysplasia (MAD).[21−23]

DCM is the most common disorder encountered at cardiovascular clinics around the world,[24] characterized by increased systolic and diastolic volumes leading to cardiac sudden death.[25] Numerous mutations of the *LMNA* gene have been uncovered via global clinical studies with patients afflicted with DCM.[23,26−31] However, it is important to stress that no underlying mechanism connecting mutant lamin A to the pathophysiology of the disease is known to date. On the basis of such a recent study of the identification of novel mutations in the *LMNA* gene among 27 Italian families whose proband was diagnosed with DCM,[32] we have focused on a structure−function analysis of three such mutations, K97E, E161K, and R190W. The rationale behind our study is understanding how the mutations in the rod domain of the protein influence the overall structure and hence its self-association behavior at the molecular level. Various studies of samples from laminopathy-afflicted patients[33] as well as with ectopic expression of mutant proteins in cultured cell lines[30,34,35] have shown the formation of misshapen nuclei with herniations, blebs, intranuclear foci, and aggregates with various sizes and distribution patterns. This can be attributed to the fact that mutations in lamin A could perturb self-association or homotypic interaction, heterotypic interactions with lamin B1 and B2, interactions with NE-associated and nucleoplasmic proteins, and interactions with chromatin in all possible manners.

In this work, we investigated the morphology of the transfected nuclei for both wild type and mutant proteins tagged with EGFP. Using confocal microscopy, the transfected nuclei were shown to possess aggregates of different sizes and distributions despite having no gross abnormality in the nuclear envelope. Aggregate formation thus seemed to be a major hallmark of these mutants that has been corroborated by light scattering experiments with the purified proteins where the size distribution of the aggregates varied significantly from the wild type to mutants. Morphometric analyses were followed by CD and fluorescence spectroscopic studies of the purified proteins. These studies permitted us to make a comparative analysis of the secondary and tertiary structures of the proteins as a sequel to mutations in the wild type. We also performed isothermal titration calorimetry for the first time to compare the enthalpy changes associated with the self-assembly process of lamin A and its mutants. Taken together, this report aimed to provide a molecular basis of the difference in the structural properties and hence oligomerization of the wild type protein from the three mutants, known to be present in DCM afflicted patients.

EXPERIMENTAL PROCEDURES

Site-Directed Mutagenesis. Site-directed mutagenesis was performed on pET-human lamin A and pEGFP-human lamin A (gift from R. D. Goldman, Northwestern University, Feinberg School of Medicine, Chicago, IL) to obtain mutations K97E, E161K, and R190W using *Pfu* polymerase (Fermentas) and two primer sets each containing the mutations, specific for two different templates: K97E_sense, 5′-gactcagtagccgaggagcgcgc-cc-3′; K97E_antisense, 5′-gggcgcgctcctcggctactgagtc-3′; E161K_sense, 5′-gcacgctggagggcaagctgcatgatctg-3′; E161K_antisense, 5′-cagatcatgcagcttgccctccagcgtgc-3′; R190W_ sense, 5′-atgagatgctgcggtgggtggatgctgag-3′; R190W_antisense, 5′-ctcagcatccacccaccgcagcatctcat-3′. The cycling conditions were as follows: 95 °C for 1 min and 18 cycles of 95 °C for 30 s, 65 °C for 30 s, and 72 °C for 14 min, followed by 15 min at 72 °C. Reaction products were treated with DpnI (Biolabs) for 5 h at 37 °C and transformed in XL1Blue (Stratagene) cells for plasmid isolation using the miniprep/maxiprep kit (Qiagen). Mutants were confirmed by sequencing.

Expression and Purification of Protein. Wild type human prelamin A/full-length lamin A (664 amino acids) and its mutant proteins mentioned above were expressed in a heterologous fashion in BL21(DE3) pLysS (Novagen) from pET-human LA. Proteins were overexpressed in TB, 2× YT, and/or LB broth (Himedia) as applicable and supplemented with ampicillin, chloramphenicol, and kanamycin (USB Corp.). Protein expression was induced at an OD_{600} of 0.5−0.6 by 2 mM IPTG (Himedia) for 2 h. Cell pellets were lysed and washed as described by Moir et al.,[36] and all the steps were performed in the presence of protease inhibitor cocktail (Sigma). PMSF (1 mM, Sigma) was used during and after induction for R190W. The proteins were purified to near homogeneity using a Mono S5/50 GL column (GE Healthcare). Protein fractions were eluted in 6 M urea, 25 mM Tris-HCl (pH 8.5), 250 mM NaCl, and 1 mM DTT. Proteins were renatured by being dialyzed in a stepwise manner from 6 M to the final protein buffer (PB) composed of 25 mM Tris-HCl (pH 8.5), 250 mM NaCl, and 1 mM DTT at room temperature in steps of two using Slide-A-Lyzer-Mini dialysis units (Thermo Scientific) with a 10000 molecular weight cutoff Bradford reagent (Bio-Rad) and/or the BCA kit (Pierce) used for protein quantification in a Cecil 7500 UV−vis or Nanodrop2000 spectrophotometer (Thermo Scientific). Prior to all biophysical studies reported here, the buffers and proteins were centrifuged at 13000 rpm at 25 and 4 °C, respectively, for 30 min and filtered through Milex Syringe filters (0.22 μm) (Milipore) to eliminate any amorphous aggregates. The concentrations of the protein were checked before and after the physicochemical studies and found to be same within the permissible range of error in estimation (±5%).

Cell Culture and Cell Cycle Analysis. HeLa cells were cultured in Dulbecco's modified Eagle's medium (DMEM) (Himedia), supplemented with 10% fetal bovine serum (Gibco) and 5% penicillin/streptomycin (Sigma), and maintained in a humidified incubator at 37 °C in 5% CO_2. Transfections with pEGFP-human LA (EGFP-wt LA) and mutant constructs were conducted using Lipofectamine 2000 (Invitrogen) in accordance with the manufacturer's protocol at early passages (5−7) having 80−85% confluency and were kept in culture for 36−48 h. The transfection efficiency was quantified based on visualization of GFP fluorescence in an inverted fluorescence microscope. Cell synchronization at the G_0/G_1 stage was achieved by serum starvation for 72 h. Transfected HeLa cells were harvested and washed twice with phosphate-buffered saline (PBS). Cell pellets were collected by centrifugation at 250*g* for 5 min at room temperature; cells were resuspended in PBS and fixed in 70% ethanol for 2 h. Cells were pelleted by centrifugation at 250*g* for 5 min at room temperature, washed again with PBS, and finally stained with a propidium iodide (PI) solution (final concentration of 50 μg/mL). Cells were analyzed on a BD FACS Aria III instrument (BD Bioscience) equipped with a 488 nm laser system. Cell aggregates and apoptotic cells were excluded from analysis by doublet discrimination. Cell cycle analysis was conducted using BD FACS Diva software; a total of 20000 cells (approximately) were scored, and 200−300 cells were scored for EGFP positive cells. Each experiment was repeated twice.

Immunofluorescence Analysis. Cells transfected with EGFP-wt LA and mutant constructs were grown on glass coverslips for 36−48 h, fixed in 4% paraformaldehyde for 15 min at room temperature, followed by permeabilization for 15 min with 0.1% Triton X-100 in PBS at room temperature, and stained with Vectashield (Vector Laboratories). Fluorescence images were acquired with an LSM510 confocal microscope (Carl Zeiss) with oil immersion objective lenses (63×). Images were processed using Axiovision version 4.8 (Carl Zeiss).

Western Blot Analysis. Transfected HeLa cells were lysed in RIPA buffer. Whole cell lysate was quantified for protein estimation with the BCA kit using a Nanodrop 2000 spectrophotometer (Thermo Scientific), and equal amounts of protein (90 μg) were loaded and resolved in 10% sodium dodecyl sulfate−polyacrylamide gel electrophoresis (SDS−PAGE). Separated bands were transferred to a nitrocellulose membrane (Millipore) with a 0.45 μM pore size. Nonspecificity was blocked with 5% NFDM in PBS containing 0.1% Tween 20. The membrane was probed with a mouse monoclonal anti-human lamin A+C (JoL2) antibody (Upstate Millipore) at a dilution of 1:100, a rabbit monoclonal anti-GFP primary antibody (Cell Signaling) at a dilution of 1:200, and mouse monoclonal anti-human β-actin (Sigma Aldrich) used as a loading control at a dilution of 1:1000, washed with PBS containing 0.1% Tween 20, and subsequently treated with stabilized peroxidase-conjugated secondary goat anti-mouse or anti-rabbit (H+L) antibody (Thermo Scientific) at dilutions between 1:250 and 1:2000. Super Signal West Pico Chemiluminescent Substrate (Thermo Scientific) was used to develop chemiluminescence, and the chemiluminescence was imaged using Kodak Medical X-ray Film. Purified lamins obtained from heterologous expression in bacteria were similarly blotted using optimal primary and secondary antibody dilutions. Blots were repeated in at least triplicate if not otherwise mentioned.

Statistical Analyses. The number of aggregate-containing nuclei for each mutant construct was compared with corresponding wt LA counts using a two-tailed χ^2. InStat 3 (Graphpad Software, Inc., La Jolla, CA) statistical software[30] was used for all analyses (Table 1).

Table 1. Statistical Analyses of Wild Type and Mutant Constructs[a]

LMNA construct	total no. of transfected cells[b]	aggregates (% *n*)	*P*, test
wt LA	1621 ± 36	0.25	not applicable
K97E	996 ± 41	8	<0.0001, CS
E161K	387 ± 10	21	<0.0001, CS
R190W	522 ± 20	9	<0.0001, CS

[a]CS indicates a χ^2 test; *n* indicates the number of data collected. [b]Pooled data were derived from at least three independent experiments.

Steady State Fluorescence Spectroscopy. Fluorescence emission spectra at an excitation wavelength of 295 nm were recorded in a Perkin-Elmer LS 55 luminescence spectrometer at 25 °C using quartz cuvettes with a 1 cm path length. For both excitation and emission, slit widths were kept at 5 nm. The emission spectra were normalized with respect to that of *N*-acetyl-L-tryptophanamide (Sigma Aldrich) dissolved in protein buffer at 25 °C corresponding to the molar content of the Trp residues in the protein(s); the absorbance values of proteins at 340 nm were in the range of 0.01−0.03. It eliminated the necessity for correction due to inner filter effects.

4,4′-Bis(1-anilinonaphthalene 8-sulfonate) (bis-ANS), obtained from Molecular Probes Inc., was dissolved in freshly distilled dimethyl sulfoxide (Fluka). The concentration of this solution was determined in methanol in a Cecil 7500 UV−visible spectrophotometer (ε_{395} in methanol = 23000 M^{-1} cm^{-1}).[37] The emission spectra of bis-ANS (6 μM) were recorded at an excitation wavelength of 399 nm. The excitation and emission slit widths were 5 nm. Corrections for the inner filter effect were not employed as the absorbance values did not exceed the limiting value of 0.05 in the scan range of 430−590 nm.

Circular Dichroism (CD). Far-UV CD spectra of the proteins over a concentration range of 84 nM to 4 μM in PB were recorded at 25 °C in a Jasco J-720 spectropolarimeter with a quartz cuvette with a path length of 1 mm. Near-UV CD spectra in the range of 250−300 nm were recorded at 25 °C in a quartz cuvette with a path length of 1 cm to examine the effect of mutations on the tertiary structures of human wt LA and the three mutants. The protein solutions were filtered and centrifuged, and the concentrations were checked before and after the CD experiments.

Isothermal Titration Calorimetry (ITC). The thermodynamics of the self-association process of lamin A proteins was studied by isothermal titration calorimetry (ITC) in a Microcal ITC200 microcalorimeter. Two approaches were adopted to study the process. In the first method, small aliquots of the protein were added from a concentrated stock solution in the syringe to a very dilute solution (50 nM) of the protein; 12.4 μL of a 35 μM protein solution in PB was added from a 40 μL syringe to a cell (volume) containing 50 nM protein in the same buffer in aliquots of (1 × 0.4 + 12 × 1) μL at 25 °C so that the final concentration of the proteins was 1.5 μM. The stirring speed of the syringe was 200 rpm. In the control experiment, the syringe contained the buffer without the protein.

In the second approach, a fixed volume of the concentrated solution was added to a dilute solution (50 nM) of the protein in a single-injection method (SIM). This approach was employed to estimate the associated thermodynamic parameters and the degree of oligomerization of lamin A proteins at higher concentrations. Twenty microliters of the proteins from similar stock solutions was added so that the resulting concentration in the cell became 3.5 μM at 25 °C. In the single-injection method, the stirring speed was kept at 400 rpm. Stock solutions of the proteins were degassed and centrifuged for 30 min at 25 °C prior to experimentation. The thermograms so obtained from the single-injection method were fit using the single set of binding sites model of the Levenberg−Marquardt nonlinear least-squares curve fitting algorithm, built into the MicroCal LLC software. The protein (50 nM), thought to be in the deoligomerized state, was considered as the macromolecule (bulk concentration M_t in active cell volume V_0), to which 35 μM proteins bound, considered as the ligand with bulk (X_t) and free concentrations ([X]) in active cell volume V_0. The apparent association constant (K_a) is given by

$$K_a = \frac{\theta}{(1-\theta)[X]}$$

where θ is the fraction of sites occupied by the ligand. The bulk concentration of the ligand is given by

dx.doi.org/10.1021/bi400337t | *Biochemistry* 2013, 52, 4229−4241

$$X_t = [X] + n\theta M_t$$

where n is the number of binding sites. The total heat content of the solution present in V_0 is

$$Q = n\theta M_t \Delta H V_0$$

where ΔH is the molar heat of binding. Considering the change in volume, ΔV_i accompanied by the ith injection, the associated heat released is given by

$$\Delta Q_i = Q_i + \frac{dV_i}{V_0}\left(\frac{Q_i + Q_{i-1}}{2}\right) - Q_{i-1}$$

The binding entropy was obtained from

$$\Delta G = -RT \ln K_a = \Delta H - T\Delta S$$

where R is the universal gas constant and T is the temperature at which the experiment was performed.

Dynamic Light Scattering (DLS). Dynamic light scattering measurements were performed with lamin A proteins in PB at 25 °C on a Zetasizer Nano S particle analyzer (Malvern Instruments) equipped with a 4 mW He−Ne laser (632.8 nm) as the light source, the detector being placed at a fixed angle of 173°. A correlation curve to obtain the Stokes−Einstein diffusion coefficient (D) was generated from the intensity autocorrelation function given by $G(\tau) = A[1 + B\exp(-2\Gamma\tau)]$, where G is the correlation coefficient, A is the amplitude of the correlation function, and B is the baseline. $\Gamma = D\cdot\mathbf{q}^2$, where $\mathbf{q}$ is the scattering vector. Cumulant analysis of the correlation curve[38] was used to obtain the intensity percentage statistical distribution by the built-in software and the mean hydrodynamic diameters at the position of maximal intensity (percent) obtained from it.

RESULTS

Protein Expression and Purification. Heterologous protein overexpression was standardized in 2× YT medium by adjustment of the IPTG concentration to 2 mM for induction. For the sake of clarity, it should be emphasized that we would refer to the wild type full-length lamin A as wt LA and the mutants as K97E, R190W, and E161K in the subsequent experiments. The mutant R190W protein showed rapid degradation on the gel compared to the wild type and other mutants, which was circumvented by growing the cells in LB and including 1 mM PMSF from induction onward. Heterologous expression of human lamin A and the mutants from BL21DE3 cells was quite robust as shown in Figure 1B. Proteins were purified by using a cation exchange column to near homogeneity (>95% purity). For all subsequent biophysical experiments, proteins of similar purity were used. During renaturation of the protein by stepwise removal of urea, R190W showed a maximal propensity for precipitation. Equal amounts of proteins were blotted with the anti-lamin A antibody that showed robust and clean bands. The homogeneity of the preparation was of utmost importance as we would conclude from the following experiments that the results did not stem from any artifacts of impurity but solely from the protein of interest.

Morphological Analysis of Transfected Nuclei. Cultured HeLa cells between passages 5 (P5) and 7 (P7) were routinely used to study and compare nuclear morphology following transfection with Lipofectamine 2000. The cells transfected with EGFP-wt LA exhibited a uniform rim staining and a characteristic nucleoplasmic distribution. A few transfected cells of no statistical significance showed the presence of small aggregates. These nuclear aggregates were also visualized in nontransfected HeLa cells stained for endogenous lamin A/C (unpublished data). Such structures have been reported by many groups and correspond to functionally different types of intranuclear structures.[39−42] In the lamin A mutant-transfected cells, significant aggregates of varying sizes and numbers were observed along with a marked reduction in the extent of rim staining. Similar results were reported earlier in COS7 cells transfected with GFP-LA mutants like R89L, R166P, R190Q, E203K, I210S, L215P, and R471H.[30] Formation of intranuclear foci had been reported in HeLa cells transfected with the DCM mutant of lamin A N195K.[34] Figure 2 represents a comparison between the wild type lamin A and representative mutant-transfected cells. The transfection efficiency was between 50 and 60% for the wild type construct and between 20 and 25% consistently in the case of the mutants. The size and extent of aggregate formation among the transfected cells were quantified manually using an epifluorescence microscope by a person blinded to the experimental details and seem to be distinctly different across the mutants. The percentage of aggregates scored highest in the case of EGFP-E161K (Table 1).

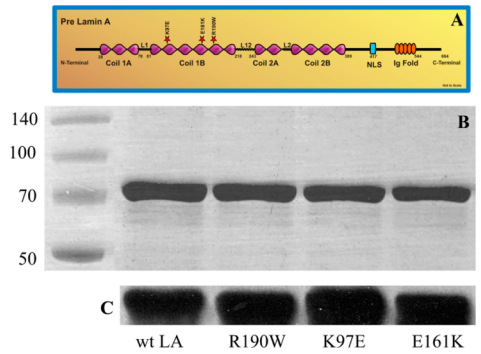

Figure 1. Overexpression of wt human lamin A and its mutants. (A) Schematic representation of human full-length lamin A. (B) FPLC column-purified proteins were resolved via 10% SDS−PAGE and Coomassie stained. (C) Immunoblot analysis of the purified proteins by JoL2.

The size of the aggregates in terms of area was calculated using ImageJ and is shown in Figure 2D. Quantifications were based on measurements from experiments conducted in triplicate using approximately 200 nuclei each time. EGFP-K97E transfected nuclei showed the presence of a maximal number of giant aggregates. In retrospect, the giant aggregates had been reported previously only in cells ectopically expressing lamin C;[43,44] subsequently, Cowan et al.[30] have shown the presence of the giant aggregates in their studies with the COS7 cell line transfected with idiopathic and familial dilated cardiomyopathy-linked mutants. The levels of expression for EGFP-wt LA and its mutants were comparable as validated by Western blot analysis conducted in quadruplicate. We further calculated the form factor (FF) of the nuclei using the formula $[4\pi(\text{area})]/(\text{perimeter}^2)$, which equals 1 for a perfectly circular perimeter and <1 for a geometry deviating from a perfect circle.[45] For these measurements, 200 nuclei were similarly scored from three replicates of experiments using ImageJ, and the results are represented in Figure 2E. Hence, we speculate that these mutations probably do not perturb the protein−protein interaction of lamin A/C and NE-associated protein like emerin, LAP 2α, MAN 1, etc., although that needs to be shown in a separate study and is beyond the

dx.doi.org/10.1021/bi400337t | Biochemistry 2013, 52, 4229−4241

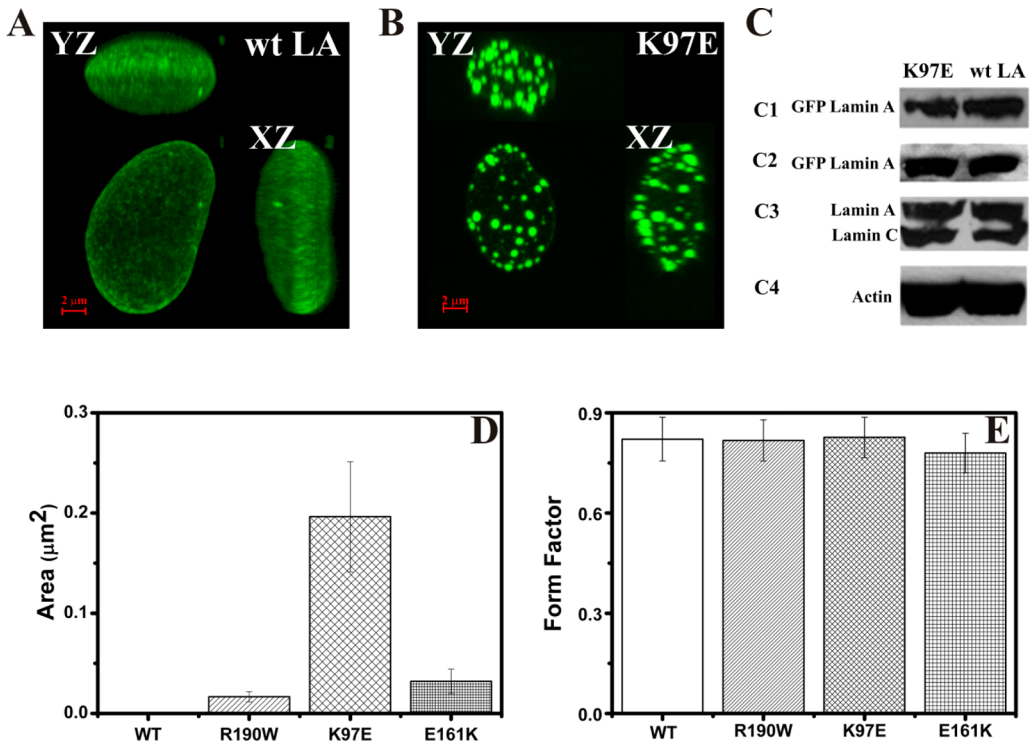

Figure 2. Comparison of the nuclear aggregates and nuclear morphology among the wt and mutant proteins. HeLa cells were transfected with (A) pEGFP-human LA for 48 h and (B) pEGFP-human K97E LA for 48 h. Cells were fixed as described and mounted with Vectashield. Maximal projections of *z*-sections and *x*−*z* and *y*−*z* projections are shown as described above. The pEGFP-human K97E LA-transfected nucleus shows distinct nuclear lamin aggregates and subsequent perturbation of nuclear rim staining compared to that of the wt. The scale bar is 2 μm. (C) Representative immunoblot analysis of EGFP-wt LA and EGFP-K97E, with actin being used as a loading control: (C1) with anti-GFP showing ectopically expressed fusion protein, (C2 and C3) with Jol2 showing ectopically expressed fusion protein and endogenous lamin A/C, respectively, and (C4) with anti-β-actin. A comparable level of expression of EGFP-lamin was observed in wt LA and K97E. (D) Variation in aggregate size among EGFP-wt LA and its mutants. The size represented in area (square micrometers) is the largest for EGFP-K97E, showing giant aggregates as compared to other mutants. (E) Form factor calculation for the nuclei transfected with EGFP-wt LA and its mutants showed no variation, suggesting not much deviation from a near perfect circular shape. Error bars representing the standard deviation were calculated from ~200 nuclei each for each set of triplicate experiments.

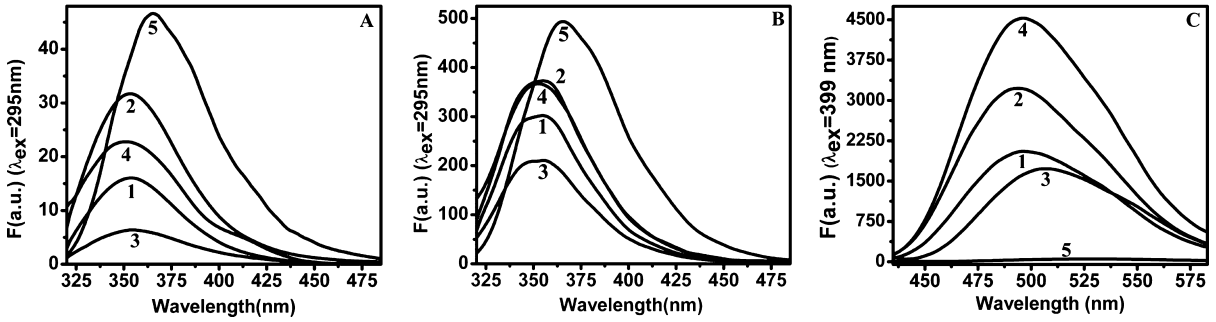

Figure 3. (A and B) Fluorescence emission spectra (λ_{ex} = 295 nm) of wild type and mutant lamin A proteins and NATA: (A) 0.4 μM lamin A proteins and 1.6 μM NATA and (B) 4 μM lamin A proteins and 16 μM NATA [(1) wt LA, (2) R190W, (3) K97E, (4) E161K, and (5) NATA] in 25 mM Tris-HCl buffer (pH 8.5) containing 250 mM NaCl and 1 mM DTT at 25 °C. (C) Fluorescence emission spectra (λ_{ex} = 399 nm) of 6 μM bis-ANS alone (5) and in presence of the mutant and wild type proteins (6 μM) in the same buffer at 25 °C [(1) wt LA, (2) R190W, (3) K97E, and (4) E161K].

scope of this paper. However, on the basis of previous findings by Shumaker et al.,[46] it is quite possible that these nucleoplasmic lamin A aggregates might act as sequestration sinks for molecules like PCNA that would eventually be reflected in delayed entry into the S phase. To answer this question, a synchronized HeLa cell culture was transfected with wild type as well as mutant constructs. However, no changes were observed for the mutants in the cell cycle stages compared to the wild type (data not shown).

Fluorescence Spectra of Wild Type and Mutant Proteins To Compare Their Structures. Panels A and B of Figure 3 show the steady state fluorescence spectra of wild type and mutant lamins at low (0.4 μM) and high (4 μM) concentrations. Each spectrum was normalized using *N*-acetyl-L-tryptophanamide (NATA), where the Trp residue is fully exposed. Comparison with NATA highlighted the following features. (i) The emission peaks were blue-shifted for all proteins. (ii) At a low concentration (0.4 μM), the extent of the

dx.doi.org/10.1021/bi400337t | *Biochemistry* 2013, 52, 4229−4241

blue shift depended on the nature of the mutation, being maximal for E161K. In case of K97E, the increase in protein concentration to 4 μM led to a blue shift in the emission maximum. In contrast, a similar increase in concentration led to a red shift for E161K (Table 2). The peak emission intensity

Table 2. Fluorescence Emission Maxima of Wild Type and Mutant Proteins as a Function of Concentration

	λ_{max} (nm)	
protein	0.4 μM	4 μM
wt LA	355	355
R190W	357	355
K97E	358	356
E161K	350	353
NATA	365	365

was also dependent on the nature of the mutation. It may be noted that the four Trp residues are located in the C-terminal tail domain and the mutations at the rod domain are distant from these residues. Therefore, differences in the peak position and intensity of Trp residue(s) in the proteins as a consequence of point mutations in the protein can be attributed to differences in secondary and/or tertiary structure. There are reports that suggest that lamin A undergoes aggregation at higher concentrations.[47] In our case, the hydrophobic environment of the Trp residues in the aggregated forms led to the enhanced quantum yield.

Nature of the Hydrophobic Pockets of the Self-Associated Proteins. We conducted a comparison of the hydrophobic pockets among wild type and mutant lamin A proteins in the aggregated forms by a fluorescent reporter, bis-ANS. Bis-ANS, the widely used probe for hydrophobic pockets of proteins,[48] showed an increase in fluorescence along with blue shift upon addition of the wild type and three lamin A mutants (Figure 3C and Table 3). Among the wild type and the

Table 3. Increases in the Intensity and Blue Shifts in the Emission Spectra of Bis-ANS (6 μM) in the Presence of Wild Type and Mutant Lamin A (6 μM)

system	λ_{max} (nm)	F (arbitrary units) at λ_{max}
bis-ANS	530	49 ± 1
bis-ANS with wt LA	497	2052 ± 6
bis-ANS with R190W	494	3224 ± 7
bis-ANS with K97E	507	1730 ± 4
bis-ANS with E161K	496	4530 ± 8

three mutants, we noticed a significant difference in the extent of the blue shift and an increase in emission intensity. At equimolar concentrations of the lamin A proteins, the intensity increased by 42- and 31-fold and the emission maxima shifted by 33 and 23 nm for wt LA and K97E, respectively. On the other hand, in the cases of R190W and E161K, the increase in the fluorescence intensity of bis-ANS was 66- and 92-fold and the wavelength shifts were 36 and 34 nm, respectively (Table 3). The differences in the emission maxima and intensity values of the reporter molecule, bis-ANS, in the presence of different lamins indicated that the hydrophobic pockets thus formed in the proteins at higher concentrations were significantly different. This effect could originate from the difference in the tertiary structures of the wild type and mutant proteins in their aggregated forms at higher concentrations.

CD Spectroscopic Studies Demonstrate the Perturbation in the Secondary and Tertiary Structures of Lamin A Caused by DCM Mutations. Fluorescence-based experiments suggested differences in the secondary and/or tertiary structures as a sequel to mutations in wild type lamin A. To support this observation, we used far-UV and near-UV CD spectroscopy to look for any structural perturbations arising from mutations at the secondary and/or tertiary level. Keeping in mind the earlier reports of coiled-coil formation via self-association of the lamin A monomers,[47] we recorded far-UV CD spectra of full-length proteins in the concentration range of 0.084−4 μM. All spectra were normalized to molar ellipticity values. Panels A and B of Figure 4 depicting the far-UV CD spectra at two concentrations reflected the preponderance of helical structure with the following features. At the lowest concentration, the wild type lamin had a backbone structure different from that of the three mutants. On the other hand, the mutants among themselves also had nonoverlapping spectra. A reciprocal relationship between the molar ellipticity of the lamins and their input concentrations was clearly indicative of the formation coiled-coil structure as present in dimers and even higher-order structures resulting from the association of the coiled-coil dimers. Ellipticity versus concentration curves (Figure 4D) were different for the wild type protein and the three mutants, further highlighting the variation of the backbone structure upon the nature of amino acid substitutions. The proposition of difference in the tertiary structures of the wild type lamin and the three point mutants was also supported by a comparison of their side chain CD spectra in the near-UV region (Figure 4C).

The alteration in tertiary structure demonstrated above by fluorescence and near-UV CD spectra might be a sequel to the difference in their secondary structures. Figure 4D shows the plot of molar ellipticity at 222 nm against the varying concentrations of wild type and mutant proteins. Inflection points in the plot for wild type and mutant lamin A were different, suggesting a difference in the oligomerization constants. It was evident from the graph that the proteins remained in one state of association up to a certain protein concentration (Table 4). Above this concentration (inflection point), which was dependent upon the nature of the protein, the proteins started undergoing further oligomerization. The ratio of the molar ellipticity values at 222 and 208 nm was used as a diagnostic tool to improve our understanding of the nature of the helix.[49] This parameter was plotted to examine the concentration-dependent nature of helicity in the proteins. The plot of the ratio of the observed ellipticity at 222 and 208 nm as a function of concentration of wild type and mutant proteins (Figure 4E) showed a distinct trend for E161K, where the ratio increased from 0.54 to 0.93 with an increasing concentration, which can be attributed to the formation of a coiled-coil structure from an isolated helix;[49] for the rest of the proteins, the helicity was altered, but in a dissimilar fashion. Here, the ratios decreased with an increasing concentration and always remained above a value of 0.98, suggesting the consistent presence of coiled-coil structure. The difference could be ascribed to two plausible factors. The nature of the helix in terms of residues per turn and length was different in the case of E161K. Alternately, the angle between the transition dipoles giving rise to the bands at 222 nm ($n \rightarrow \pi^*$) and 208 nm ($\pi \rightarrow \pi^*$) was radically different in the case of the bundled cylindrical forms of the E161K oligomers. These data are not sufficient to

dx.doi.org/10.1021/bi400337t | Biochemistry 2013, 52, 4229−4241

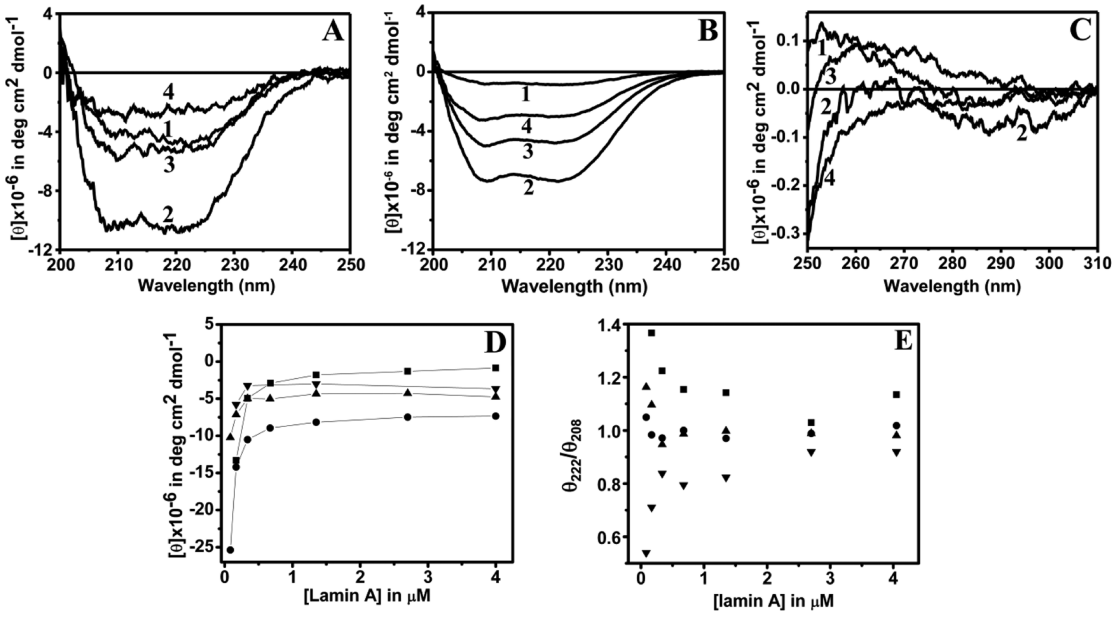

Figure 4. Far- and near-UV CD spectra of wild type and mutant lamin A. Far-UV CD spectra of (A) 0.4 μM lamin A and (B) 4 μM lamin A [(1) wt LA, (2) R190W, (3) K97E, and (4) E161K] in 25 mM Tris-HCl buffer (pH 8.5) containing 250 mM NaCl and 1 mM DTT at 25 °C. The spectra were not smoothed. (C) Near-UV CD spectra of lamin A [(1) wt LA, (2) R190W, (3) K97E, and (4) E161K] measured under the same conditions. (D and E) Plots of the molar ellipticity at 222 nm (D) and the ratio of θ_{obs}(222 nm) to θ_{obs}(208 nm) (E) for wild type and mutant lamin A [(■) wt LA, (●) R190W, (▲) K97E, and (▼) E161K] as a function of input concentration.

Table 4. Inflection Points in the Plot of Molar Ellipticity vs Concentration for Wild Type and Mutant Lamin A

	wt LA	R190W	K97E	E161K
inflection point (μM)	0.72 ± 0.06	0.53 ± 0.03	0.66 ± 0.03	0.58 ± 0.04

distinguish between them. However, we have discussed it from another perspective in the Discussion.

Energetics of the Self-Association of Wild Type and Mutant Proteins. Self-association toward supramolecular assembly is a common phenomenon for the intermediate filament assembly. In this report, with the help of different spectroscopic techniques like fluorescence and CD, we established that single-amino acid mutations in lamin A could

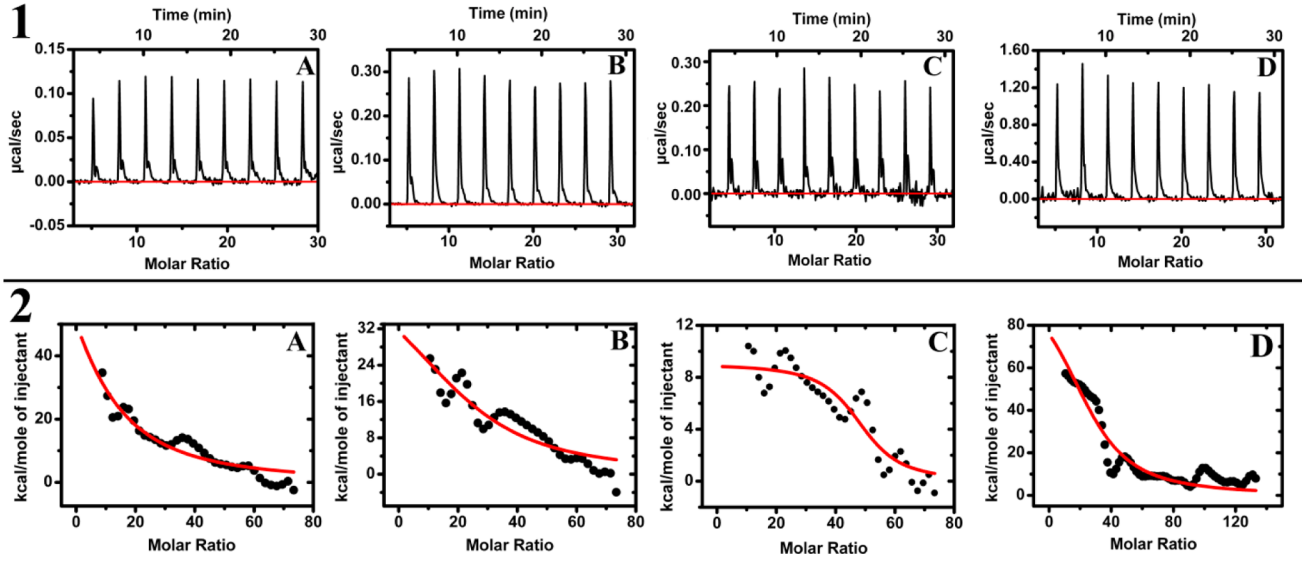

Figure 5. Isothermal calorimetric titration for the dissociation−association equilibria of aggregated wild type lamin A and its three mutants. Panel 1 represents the injections for dilution of 35 μM protein (in syringe) to a 1.5 μM sample (final concentration in the cell): 12.4 μL of a 35 μM protein solution in 25 mM Tris-HCl buffer (pH 8.5) and 250 mM NaCl was added from a 40 μL syringe to a cell (volume of 200 μL) containing 50 nM protein in the same buffer in aliquots of (1 × 0.4 + 12 × 1) μL at 25 °C so that the final concentrations of the proteins were 1.5 μM. Panel 2 represents the fitted curves obtained via the SIM as a result of dilution of 35 μM protein (in syringe) to 3.5 μM (final concentration in the cell): 20 μL of a 35 μM protein solution was added in each case so that the resulting concentration in the cell was 3.5 μM at 25 °C. Panels A−D in each set of figures correspond to wt LA, R190W, K97E, and E161K, respectively.

dx.doi.org/10.1021/bi400337t | *Biochemistry* 2013, 52, 4229−4241

affect the overall tertiary structure of the protein, thereby affecting the process of self-association. As a sequel to these observations, we addressed the question of whether this stepwise process of self-association in the case of the mutant proteins differed from that of the wild type as far as the energetics characterizing the process is concerned. Therefore, we probed the thermodynamics of the molecular association of wild type and the mutant proteins by isothermal titration calorimetry (ITC). In the typical experimental setup, a concentrated protein stock solution in the range of 35 μM was added to the cell containing a very dilute (50 nM) protein solution. As a result, the higher-order oligomerized structure became diluted or "deoligomerized", which would then register a change in heat. Two sets of experiments were conducted for each of the four proteins. From a 35 μM protein stock solution (wild type and the mutants) were added aliquots until the final concentration of 1.5 μM corresponding to the first linear region of the CD titration profile was reached. The resultant thermograms exhibited differences in terms of the enthalpy changes. The change in the enthalpy turned out to be an endothermic process in both cases. It occurred because of the dissociation and progressive association of the oligomer in the cell as represented in the following equation:

$$L_n \rightleftharpoons n(L)$$

where n denotes the state of association and L symbolizes the monomeric lamin A protein.

Nonoverlapping and distinct characteristic profiles (Figure 5) for the wild type and mutant proteins indicated that the enthalpy of dissociation of the oligomeric species in the calorimetric cell depended upon the nature of the mutation. To determine the oligomerization process, in particular the number of lamin monomers present in the higher-order structure as manifested in the CD spectra and the corresponding titration profiles (in the region beyond the break point), we conducted the ITC titrations in the SIM. The stock solution (35 μM) was dropped in a single injection so that the final concentration became 4 μM. The raw profiles are given in the Supporting Information, and the fitted curves for obtaining the relevant parameters are shown in panel 2 of Figure 5. Such analysis provided the degree of oligomerization in the native state for the four lamin proteins used along with relevant thermodynamic parameters. Table 5 shows that the oligomerization was entropy driven, implying the role of water and configurational entropy of the protein in the process. The N value of 8 for the wild type is consistent with the previous reports of an octameric state of self-association of wild type lamins.[16] Another notable feature was the increase in the number of monomeric proteins in the oligomers of the mutants, the maximal value being 48 for K97E. Similarly, the self-association constant was also highest for K97E. The other two mutants, E161K and R190W, also associated more strongly than the wild type.

Table 5. Thermodynamic Parameters Obtained via Isothermal Titration Calorimetry in the Single-Injection Mode for Wild Type and Mutant Proteins

protein	N	ΔH (kcal mol^{-1})	ΔS (cal mol^{-1} deg^{-1})	K_d (μM)
wt LA	8 ± 0.5	165.0 ± 8.5	581	0.97 ± 0.06
R190W	24 ± 1.5	48.5 ± 3.5	191	0.69 ± 0.03
K97E	48 ± 1.7	9.0 ± 0.5	64	0.05 ± 0.01
E161K	29 ± 4.2	103.6 ± 19.5	376	0.55 ± 0.02

Comparison of Hydrodynamic Diameters of Lamin A Protein Aggregates by Dynamic Light Scattering. Figure 6 illustrates the intensity percentage distribution for the different protein species at 4 μM. The results are summarized in Table 6. They indicate a distinct aggregation profile for E161K (Figure 6 and Table 6). In case of the wild type and other two mutants, R190W and K97E, we encountered a biphasic Gaussian distribution. The Gaussian distribution in these cases might originate from two populations corresponding to a bundled cylindrical form of the oligomer and/or mixed populations of globular oligomers with different hydrodynamic diameters (Table 6). In contrast, the presence of a single peak in the case of E161K could be ascribed to formation of a relatively homogeneous globular oligomer. The absence of peaks in the higher-diameter region of the intensity distribution curves ruled out the possibility of formation of higher-order aggregates. In addition, the low value of the polydispersity index (0.5) for all cases suggested the homogeneous nature of the system being reported here. However, DLS measurements did not permit us to ascertain the state of association of the oligomer for each protein.

DISCUSSION

Using a combination of biophysical techniques, we have shown in this report that the mutant lamin A proteins implicated in the pathogenesis of DCM possess distinct secondary and tertiary conformations compared to the wild type, which was reflected in gross localization defects in the cells. The structural studies by means of spectroscopic techniques indicated that mutations of the amino acids in rod 1B modulated the secondary and tertiary structure of the wild type protein. This is a significant observation in view of the clinical reports of patients harboring these mutations. The hallmark of the fluorescence data could be summarized to show that the electronic environment of Trp residues was grossly altered even though they were far removed from the sites of point mutations. Interestingly, all four Trp residues map in the highly structured Ig-fold domain in the tail region. In other words, the tertiary structure of the mutant proteins was altered as a sequel to the point mutations in the rod domain. Such an alteration in tertiary structure might be due to a change in the secondary structures of the helical domains that, in turn, would be bent in a fashion to be closest to the unstructured globular tail domain. Therefore, there could be a likelihood of spatial overlap of the tail domain on part of the rod. The difference in the tertiary structures of the lamin proteins was also corroborated by their different near-UV CD spectra. Far-UV CD spectral studies of the proteins as a function of concentration showed that monomeric forms of the wild type and mutant proteins, presumably present at low concentrations, had different degrees of helical, sheet, and random-coil forms. Plots of the variation of θ_{222} as a function of protein concentration yielded curves originating from aggregation of the four proteins. A decrease in the helicity with an increase in concentration turned out to be a common feature of the wild type and all three mutants. This reciprocal relationship could be ascribed to the formation of coiled-coil structure as reported earlier in the case of short peptides.[49] Formation of the coiled-coil structure of lamins beyond a certain concentration corresponded to the break points in the plots of molar ellipticity versus concentration. This feature, though counterintuitive, was checked by following the process in both

dx.doi.org/10.1021/bi400337t | Biochemistry 2013, 52, 4229−4241

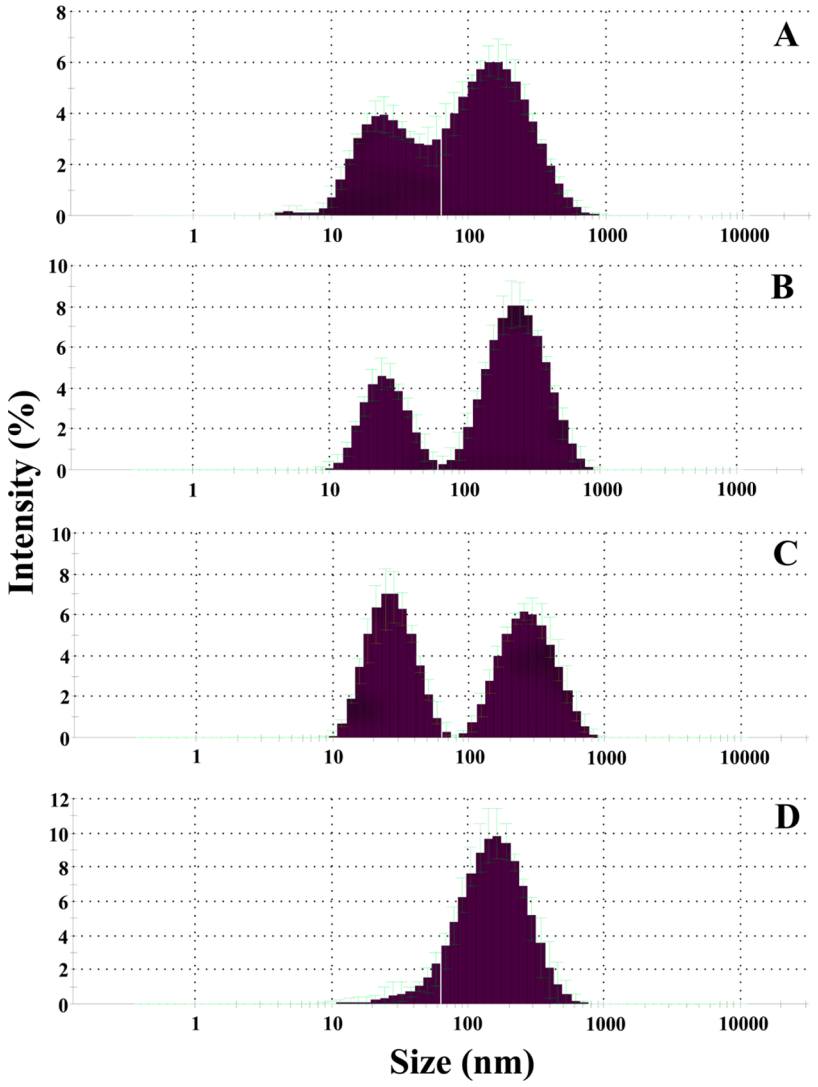

Figure 6. Intensity percentage statistical distribution of wild type and mutant lamin A proteins: (A) wt LA, (B) R190W, (C) K97E, and (D) E161K. Individual proteins (4 μM) in 25 mM Tris-HCl (pH 8.5), 250 mM NaCl, and 1 mM DTT were used for the experiments at 25 °C under identical conditions.

Table 6. Hydrodynamic Diameters of Wild Type and Mutant Lamin A at the Position of Maximal Intensity (percent)

protein (4 μM)	hydrodynamic diameter (nm) at maximal intensity[a]
wt LA	23 ± 0.4 and 153 ± 0.5
R190W	24 ± 0.7 and 238 ± 0.8
E161K	164 ± 1.2
K97E	26 ± 0.9 and 255 ± 0.3

[a]Values obtained from the intensity statistical distribution (Figure 6).

directions, i.e., from lower to higher concentrations, and the converse in two separate sets of experiments that further suggested the reversibility of this self-association. The apparent decrease in the helicity of the proteins when they aggregated could be ascribed to an unfavorable antiparallel orientation[16] of the transition dipoles (n → π^* and $\pi \rightarrow \pi^*$) in the dimers and/or the proximity of the tail domain to the helical rod domain. Far-UV CD spectra were recorded from lower to higher concentrations and vice versa in two separate sets of experiments, suggesting the reversibility of self-association. Plots of the ratio of molar ellipticity values at 208 and 222 nm supported the difference in the structures of the aggregates in the case of the E161K mutant. This ratio had been reported to be an index of the nature of the helix and the coiled-coil form.[49] Interestingly, CD spectra showed a marked decrease in ellipticity for E161K compared to those of K97E and R190W. We tried to analyze the helical content of the proteins using DICHROWEB,[50,51] an online server for secondary structure analyses, but this effort failed as the values returned were quite high and not meaningful. Similar results were obtained using K2d,[52,53] one of the available algorithms supported by DICHROWEB. The classical method formulated by Cheng et al.[54] was also unsuccessfully applied to calculate the percentage of helicity of the proteins.

The results of the different calculations were highly variable, suggesting that the structure of the oligomer could not be fit into canonical coiled coils. Nevertheless, this is an interesting piece of data hitherto not presented for full-length human lamin A proteins. Previous CD data for the fragments of the protein like the Ig fold and rod 2B did not suffer from this drawback.[12,55,56] A possible hypothesis in favor of our observations would be the protein assuming a tertiary structure where the long unfolded tail might fold back on the rod domain and hence the overall helicity of the rod would be affected by

dx.doi.org/10.1021/bi400337t | *Biochemistry* 2013, 52, 4229−4241

the random-coil contribution of the tail. The explanations for these structural studies are plagued by the lack of the structure of full-length lamin A.

Probing of the hydrophobic pockets in the aggregated proteins by fluorescence reporter bis-ANS also lent further support to our proposition of the difference in their conformations arising from mutations in the wild type protein. Among all mutants, E161K stood out as possessing distinct hydrophobicity. Reversal of the charge from E to K might offer an explanation here to be the major factor to alter the interaction among the intermolecular helical domains and the intramolecular helical domain−tail interaction.

Results of ITC compared the enthalpy of the self-association process at low and high lamin A protein concentrations and probed the possible differences, if any, with those of the mutants. In agreement with the observations from other studies, the ITC results brought out the important feature that the enthalpies characterizing the self-association of the wild type and mutant lamins are different. The results shown in panel 1 of Figure 5 indicated that the equilibrium $[L_n \leftrightharpoons n(L)]$ was an endothermic process in the lower concentration range up to 1.5 μM lamin proteins. We noticed that E161K exhibited the largest change in enthalpy during the "deoligomerization" process. The distinctive nature of the self-association of the E161K mutant was also corroborated by the comparison of the DLS profiles of the four proteins. DLS profiles with low polydispersity indices (<0.5) did not support the formation of amorphous aggregates at higher lamin concentrations. The appearance of the single peak in the case of E161K could be ascribed to formation of a globular oligomer; for the three other proteins, the presence of two peaks could be due to the predominance of the cylindrical form of the oligomer or a mixed population of globular oligomers with different diameters. The ITC results from SIM experiments pointed to the important feature that K97E oligomers possessed the largest number of monomers with the highest self-association constant. This data are consistent with the cell biological effects of these mutations on the nuclear morphology, which was validated by confocal microscopy. Table 5 containing the thermodynamic parameters for the aggregation process also indicated a relatively lower ΔH value of K97E in comparison to this value for the wild type and other mutants. Although the three mutants showed the phenotype of variable size aggregate formation inside the nucleus, from morphometric analyses we found no apparent abnormality in the nuclear shape, which was reflected in the comparable form factor values. On one hand, a maximal number of aggregates was obtained in HeLa cells transfected with EGFP-E161K, whereas EGFP-K97E-transfected cells showed the phenotype of giant aggregates. Interestingly enough, a completely unrelated lamin A mutant, E145K, found in HGPS patients had been shown to exhibit lobulated nuclei,[57] which we did not observe.

The central dogma of lamin oligomerization is the formation of coiled-coil dimers that associate in a stepwise fashion to form strings and filaments, ultimately resulting in networks. Coiled coils consist of α-helices wound around each other to form a superhelical left-handed twist. Such α-helices are characterized by heptad (7 amino acids), hendecad (11 amino acids), and pentadecad or quindecad (15 amino acids) repeats.[58] Hydrophobic interactions[59] and salt bridge/electrostatic interactions[60] have been studied in great detail from a theoretical perspective and via structural data available for some vimentin and lamin fragments[14,56,61,62] (Figure 7). Residues a and d form a

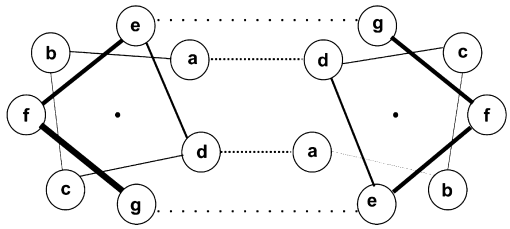

Figure 7. Cartoon representing the interactions among the polar and hydrophobic residues in an α-helical coiled-coil structure. Here residues a and d and residues e and g represent hydrophobic and oppositely charged residues, respectively. Figure adapted from ref 64.

hydrophobic seam that mediates the formation of a coiled coil that is further stabilized by electrostatic interactions and hydrogen bonding. Hydrophobic interactions lead to the assembly of the individual chain into supercoils, whereas electrostatic interactions involving residues e and g play a pivotal role in the proper alignment of the chains.[63,64] Interestingly, the mutations that are being studied here map to the 1B fragment of the rod domain. More specifically, K97E and R190W fall in the part of rod 1B that is conserved in both cytoplasmic and nuclear intermediate filament proteins. On the other hand, the E161K mutation is in the extra 42-residue segment that is not found in vertebrate cytoskeleton proteins but rather conserved in invertebrates and vertebrate lamins.

In summary, we observed notable changes in the case of E161K and K97E with respect to the wild type. The changes could be analyzed from two perspectives. One is the change in secondary and tertiary structure, and the other is the consequence that E161K showed drastic changes in its secondary and tertiary structure whereas K97E exhibited higher association constants, a fact reflected in larger aggregates in cells transfected *ex vivo*. Careful analysis of the mutated residues at positions 97, 161, and 190 revealed the corresponding positions of residues f, g, and a, respectively, as predicted by the program coils.[65,66] The results obtained from all the experiments involving the wild type and mutants bore a consensus signature with respect to mutants E161K and K97E. This is further supported by a recent report in which a host of myopathic mutations have been studied in *Lmna*$^{+/-}$ and *Lmna*$^{-/-}$ mouse embryonic fibroblast, whereby cells expressing mutants in which a residue was changed to lysine showed altered nuclear localization and solubility.[67] Therefore, it was hypothesized that mutations to lysine abrogated the proper higher-order assembly of lamin dimers as also observed in our case. Glu at position g would have a repulsive intrachain interaction with the Asp at residue i + 3 in position c in the following heptad repeat sequence. Similar interchain repulsive electrostatic interaction is expected from the two monomers aligned laterally in register. Hence, substitution of Glu with Lys at position 161 favorably abrogated the repulsion and promoted stronger electrostatic interaction between the residues i and i + 3 or i + 4 in an intrachain and interchain mode of interaction. In ITC experiments, the heat of dilution involved a maximal change in enthalpy, which again pointed to a very favorable interaction being broken by the process of chain separation or dilution. It may be worth noting that the enthalpy changes for all other mutants were not radically different from that of the wild type.

Statistical analyses of the clinical data from the probands harboring the mutations mentioned above revealed the rates of events per 100 persons per year were more or less similar for

the K97E and E161K mutations.[68] Interestingly enough, Western blot analyses of the hearts of the patients harboring the K97E mutation showed reduced lamin A/C content with an abnormal 30 kDa lamin A positive band that could be a truncation product.[26] This in turn could be true for two reasons: (a) exposure of a cryptic splice site resulting in alternative splicing of the LMNA gene and (b) structural alterations in the protein conformation facilitating an increased level of proteolytic breakdown. However, this has been a matter of speculation and not confirmed thus far. In the end, it must be emphasized that this report attempted to explain the structural consequences of three distinct point mutations in the lamin A protein. Relating the results to the functional behavior of the mutant proteins inside the cell in the disease condition would be complicated at this stage by the fact that the entire lamin proteome might be differentially regulated, hence altering the signaling conduits of the cardiomyocytes.

■ ASSOCIATED CONTENT

Supporting Information

Raw data for the injection profiles from the ITC experiments performed in the SIM. This material is available free of charge via the Internet at http://pubs.acs.org.

■ AUTHOR INFORMATION

Corresponding Author

*KSG: Biophysics Division, Saha Institute of Nuclear Physics, 1/AF Bidhannagar, Kolkata 700064, India; telephone, 91-33-2337 5345, ext. 3504; e-mail, kaushik.sengupta@saha.ac.in. DDG: Biophysics Division, Saha Institute of Nuclear Physics, 1/AF Bidhannagar, Kolkata 700064, India; telephone, 91-33-2337 5345, ext. 3114; e-mail, dipak.dasgupta@saha.ac.in.

Author Contributions

Pritha Bhattacharjee and Avinanda Banerjee contributed equally to this work.

Author Contributions

Pritha Bhattacharjee, Avinanda Banerjee, and Amrita Banerjee performed experiments. Dipak Dasgupta and Kaushik Sengupta wrote the manuscript. Kaushik Sengupta conceived the project.

Funding

We acknowledge the support from MMDDA and BARD intramural project grants from the Department of Atomic Energy, Government of India. Avinanda Banerjee acknowledges the award of a fellowship by the University Grants Commission, Government of India.

Notes

The authors declare no competing financial interest.

■ ACKNOWLEDGMENTS

We thank Dr. Shibojyoti Lahiri, Saptaparni Ghosh of the Biophysics Division of Saha Institute of Nuclear Physics, and Dr. Parijat Majumder of the Max Planck Institute of Biochemistry (Martinsreid, Germany) for insightful discussions.

■ ABBREVIATIONS

DCM, dilated cardiomyopathy; PMSF, phenylmethanesulfonyl fluoride; NATA, *N*-acetyl-L-tryptophanamide.

■ REFERENCES

(1) Cohen, M., Lee, K. K., Wilson, K. L., and Gruenbaum, Y. (2001) Transcriptional repression, apoptosis, human disease and the functional evolution of the nuclear lamina. *Trends Biochem. Sci. 26*, 41−47.

(2) Melcer, S., Gruenbaum, Y., and Krohne, G. (2007) Invertebrate lamins. *Exp. Cell Res. 313*, 2157−2166.

(3) Lin, F., and Worman, H. J. (1993) Structural organization of the human gene encoding nuclear lamin A and nuclear lamin C. *J. Biol. Chem. 268*, 16321−16326.

(4) Machiels, B. M., Zorenc, A. H., Endert, J. M., Kuijpers, H. J., van Eys, G. J., Ramaekers, F. C., and Broers, J. L. (1996) An alternative splicing product of the lamin A/C gene lacks exon 10. *J. Biol. Chem. 271*, 9249−9253.

(5) Furukawa, K., Inagaki, H., and Hotta, Y. (1994) Identification and cloning of an mRNA coding for a germ cell-specific A-type lamin in mice. *Exp. Cell Res. 212*, 426−430.

(6) Peter, M., Kitten, G., Lehner, C., Vorburger, K., Bailer, S., Maridor, G., and Nigg, E. (1989) Cloning and sequencing of cDNA clones encoding chicken lamins A and B1 and comparison of the primary structures of vertebrate A- and B-type lamins. *J. Mol. Biol. 208*, 393.

(7) Rober, R., Weber, K., and Osborn, M. (1989) Differential timing of nuclear lamin A/C expression in the various organs of the mouse embryo and the young animal: A developmental study. *Development 105*, 365−378.

(8) Stewart, C., and Burke, B. (1987) Teratocarcinoma stem cells and early mouse embryos contain only a single major lamin polypeptide closely resembling lamin B. *Cell 51*, 383.

(9) Constantinescu, D., Gray, H. L., Sammak, P. J., Schatten, G. P., and Csoka, A. B. (2006) Lamin A/C expression is a marker of mouse and human embryonic stem cell differentiation. *Stem Cells 24*, 177−185.

(10) Eckersley-Maslin, M. A., Bergmann, J. H., Lazar, Z., and Spector, D. L. (2013) Lamin A/C is Expressed in Pluripotent Mouse Embryonic Stem Cells. *Nucleus 4*, 53−60.

(11) Parry, D., Conway, J. F., and Steinert, P. M. (1986) Structural studies on lamin. Similarities and differences between lamin and intermediate-filament proteins. *Biochem. J. 238*, 305.

(12) Krimm, I., Östlund, C., Gilquin, B., Couprie, J., Hossenlopp, P., Mornon, J. P., Bonne, G., Courvalin, J. C., Worman, H. J., and Zinn-Justin, S. (2002) The Ig-like structure of the C-terminal domain of lamin A/C, mutated in muscular dystrophies, cardiomyopathy, and partial lipodystrophy. *Structure 10*, 811−823.

(13) Dhe-Paganon, S., Werner, E. D., Chi, Y. I., and Shoelson, S. E. (2002) Structure of the globular tail of nuclear lamin. *J. Biol. Chem. 277*, 17381−17384.

(14) Strelkov, S. V., Schumacher, J., Burkhard, P., Aebi, U., and Herrmann, H. (2004) Crystal structure of the human lamin A coil 2B dimer: Implications for the head-to-tail association of nuclear lamins. *J. Mol. Biol. 343*, 1067−1080.

(15) Heitlinger, E., Peter, M., Häner, M., Lustig, A., Aebi, U., and Nigg, E. (1991) Expression of chicken lamin B2 in *Escherichia coli*: Characterization of its structure, assembly, and molecular interactions. *J. Cell Biol. 113*, 485−495.

(16) Stuurman, N., Sasse, B., and Fisher, P. A. (1996) Intermediate Filament Protein Polymerization: Molecular Analysis of *Drosophila* Nuclear Lamin Head-to-Tail Binding. *J. Struct. Biol. 117*, 1−15.

(17) Ben-Harush, K., Wiesel, N., Frenkiel-Krispin, D., Moeller, D., Soreq, E., Aebi, U., Herrmann, H., Gruenbaum, Y., and Medalia, O. (2009) The Supramolecular Organization of the *C. elegans* Nuclear Lamin Filament. *J. Mol. Biol. 386*, 1392−1402.

(18) Zackroff, R. V., and Goldman, R. D. (1979) In vitro assembly of intermediate filaments from baby hamster kidney (BHK-21) cells. *Proc. Natl. Acad. Sci. U.S.A. 76*, 6226−6230.

(19) Bonne, G., Di Barletta, M. R., Varnous, S., Becane, H. M., Hammouda, E. H., Merlini, L., Muntoni, F., Greenberg, C. R., Gary, F., Urtizberea, J. A., Duboc, D., Fardeau, M., Toniolo, D., and Schwartz, K. (1999) Mutations in the gene encoding lamin A/C cause autosomal dominant Emery-Dreifuss muscular dystrophy. *Nat. Genet. 21*, 285−288.

(20) Fatkin, D., MacRae, C., Sasaki, T., Wolff, M. R., Porcu, M., Frenneaux, M., Atherton, J., Vidaillet, H. J., Jr., Spudich, S., De Girolami, U., Seidman, J. G., Seidman, C., Muntoni, F., Muehle, G.,

Johnson, W., and McDonough, B. (1999) Missense mutations in the rod domain of the lamin A/C gene as causes of dilated cardiomyopathy and conduction-system disease. *N. Engl. J. Med. 341*, 1715−1724.
(21) Broers, J., Ramaekers, F., Bonne, G., Yaou, R. B., and Hutchison, C. (2006) Nuclear lamins: Laminopathies and their role in premature ageing. *Physiol. Rev. 86*, 967−1008.
(22) Kudlow, B. A., Kennedy, B. K., and Monnat, R. J., Jr. (2007) Werner and Hutchinson-Gilford progeria syndromes: Mechanistic basis of human progeroid diseases. *Nat. Rev. Mol. Cell Biol. 8*, 394−404.
(23) Worman, H. J., and Bonne, G. (2007) "Laminopathies": A wide spectrum of human diseases. *Exp. Cell Res. 313*, 2121−2133.
(24) Richardson, P., McKenna, W., Bristow, M., Maisch, B., Mautner, B., O'Connell, J., Olsen, E., Thiene, G., Goodwin, J., Gyarfas, I., Martin, I., and Nordet, P. (1996) Report of the 1995 World Health Organization/International Society and Federation of Cardiology Task Force on the Definition and Classification of cardiomyopathies. *Circulation 93*, 841−842.
(25) Boffa, G. M., Thiene, G., Nava, A., and Dalla Volta, S. (1991) Cardiomyopathy: A necessary revision of the WHO classification. *Int. J. Cardiol. 30*, 1−7.
(26) Arbustini, E., Pilotto, A., Repetto, A., Grasso, M., Negri, A., Diegoli, M., Campana, C., Scelsi, L., Baldini, E., Gavazzi, A., and Tavazzi, L. (2002) Autosomal dominant dilated cardiomyopathy with atrioventricular block: A lamin A/C defect-related disease. *J. Am. Coll. Cardiol. 39*, 981−990.
(27) Hermida-Prieto, M., Monserrat, L., Castro-Beiras, A., Laredo, R., Soler, R., Peteiro, J., Rodriguez, E., Bouzas, B., Alvarez, N., Muniz, J., and Crespo-Leiro, M. (2004) Familial dilated cardiomyopathy and isolated left ventricular noncompaction associated with lamin A/C gene mutations. *Am. J. Cardiol. 94*, 50−54.
(28) Pethig, K., Genschel, J., Peters, T., Wilhelmi, M., Flemming, P., Lochs, H., Haverich, A., and Schmidt, H. H. (2005) LMNA mutations in cardiac transplant recipients. *Cardiology 103*, 57−62.
(29) Sylvius, N., Bilinska, Z. T., Veinot, J. P., Fidzianska, A., Bolongo, P. M., Poon, S., McKeown, P., Davies, R. A., Chan, K. L., Tang, A. S., Dyack, S., Grzybowski, J., Ruzyllo, W., McBride, H., and Tesson, F. (2005) In vivo and in vitro examination of the functional significances of novel lamin gene mutations in heart failure patients. *J. Med. Genet. 42*, 639−647.
(30) Cowan, J., Li, D., Gonzalez-Quintana, J., Morales, A., and Hershberger, R. E. (2010) Morphological analysis of 13 LMNA variants identified in a cohort of 324 unrelated patients with idiopathic or familial dilated cardiomyopathy. *Circ.: Cardiovasc. Genet. 3*, 6−14.
(31) Song, K., Dube, M. P., Lim, J., Hwang, I., Lee, I., and Kim, J. J. (2007) Lamin A/C mutations associated with familial and sporadic cases of dilated cardiomyopathy in Koreans. *Exp. Mol. Med. 39*, 114−120.
(32) Arbustini, E., Pilotto, A., Grasso, M., Marziliano, N., Serio, A., Gambarin, F., Pasotti, M., Serafini, E., Cassini, P., and Digiorgio, B. (2009) Novel human pathological mutations. Gene symbol: LMNA. Disease: cardiomyopathy, dilated with conduction defects. *Hum. Genet. 125*, 350.
(33) Vigouroux, C., Auclair, M., Dubosclard, E., Pouchelet, M., Capeau, J., Courvalin, J. C., and Buendia, B. (2001) Nuclear envelope disorganization in fibroblasts from lipodystrophic patients with heterozygous R482Q/W mutations in the lamin A/C gene. *J. Cell Sci. 114*, 4459−4468.
(34) Raharjo, W. H., Enarson, P., Sullivan, T., Stewart, C. L., and Burke, B. (2001) Nuclear envelope defects associated with LMNA mutations cause dilated cardiomyopathy and Emery-Dreifuss muscular dystrophy. *J. Cell Sci. 114*, 4447−4457.
(35) Ostlund, C., Bonne, G., Schwartz, K., and Worman, H. J. (2001) Properties of lamin A mutants found in Emery-Dreifuss muscular dystrophy, cardiomyopathy and Dunnigan-type partial lipodystrophy. *J. Cell Sci. 114*, 4435−4445.
(36) Moir, R. D., Donaldson, A. D., and Stewart, M. (1991) Expression in *Escherichia coli* of human lamins A and C: Influence of head and tail domains on assembly properties and paracrystal formation. *J. Cell Sci. 99* (Part 2), 363−372.
(37) Slavik, J. (1982) Anilinonaphthalene sulfonate as a probe of membrane composition and function. *Biochim. Biophys. Acta 694*, 1−25.
(38) Frisken, B. J. (2001) Revisiting the method of cumulants for the analysis of dynamic light-scattering data. *Appl. Opt. 40*, 4087−4091.
(39) Spann, T. P., Moir, R. D., Goldman, A. E., Stick, R., and Goldman, R. D. (1997) Disruption of nuclear lamin organization alters the distribution of replication factors and inhibits DNA synthesis. *J. Cell Biol. 136*, 1201−1212.
(40) Bridger, J. M., Kill, I. R., O'Farrell, M., and Hutchison, C. J. (1993) Internal lamin structures within G1 nuclei of human dermal fibroblasts. *J. Cell Sci. 104* (Part 2), 297−306.
(41) Machiels, B. M., Broers, J. L., Raymond, Y., de Ley, L., Kuijpers, H. J., Caberg, N. E., and Ramaekers, F. C. (1995) Abnormal A-type lamin organization in a human lung carcinoma cell line. *Eur. J. Cell Biol. 67*, 328−335.
(42) Jagatheesan, G., Thanumalayan, S., Muralikrishna, B., Rangaraj, N., Karande, A. A., and Parnaik, V. K. (1999) Colocalization of intranuclear lamin foci with RNA splicing factors. *J. Cell Sci. 112* (Part 24), 4651−4661.
(43) Broers, J. L., Kuijpers, H. J., Ostlund, C., Worman, H. J., Endert, J., and Ramaekers, F. C. (2005) Both lamin A and lamin C mutations cause lamina instability as well as loss of internal nuclear lamin organization. *Exp. Cell Res. 304*, 582−592.
(44) Sylvius, N., Hathaway, A., Boudreau, E., Gupta, P., Labib, S., Bolongo, P. M., Rippstein, P., McBride, H., Bilinska, Z. T., and Tesson, F. (2008) Specific contribution of lamin A and lamin C in the development of laminopathies. *Exp. Cell Res. 314*, 2362−2375.
(45) Mendez, M. G., Kojima, S., and Goldman, R. D. (2010) Vimentin induces changes in cell shape, motility, and adhesion during the epithelial to mesenchymal transition. *FASEB J. 24*, 1838−1851.
(46) Shumaker, D. K., Solimando, L., Sengupta, K., Shimi, T., Adam, S. A., Grunwald, A., Strelkov, S. V., Aebi, U., Cardoso, M. C., and Goldman, R. D. (2008) The highly conserved nuclear lamin Ig-fold binds to PCNA: Its role in DNA replication. *J. Cell Biol. 181*, 269−280.
(47) Aebi, U., Cohn, J., Buhle, L., and Gerace, L. (1986) The nuclear lamina is a meshwork of intermediate-type filaments. *Nature 323*, 560−564.
(48) Takashi, R., Tonomura, Y., and Morales, M. F. (1977) 4,4′-Bis(1-anilinonaphthalene 8-sulfonate) (bis-ANS): A new probe of the active site of myosin. *Proc. Natl. Acad. Sci. U.S.A. 74*, 2334−2338.
(49) Lau, S., Taneja, A., and Hodges, R. (1984) Synthesis of a model protein of defined secondary and quaternary structure. Effect of chain length on the stabilization and formation of two-stranded α-helical coiled-coils. *J. Biol. Chem. 259*, 13253−13261.
(50) Whitmore, L., and Wallace, B. (2004) DICHROWEB, an online server for protein secondary structure analyses from circular dichroism spectroscopic data. *Nucleic Acids Res. 32*, W668−W673.
(51) Whitmore, L., and Wallace, B. A. (2007) Protein secondary structure analyses from circular dichroism spectroscopy: Methods and reference databases. *Biopolymers 89*, 392−400.
(52) Andrade, M., Chacon, P., Merelo, J., and Moran, F. (1993) Evaluation of secondary structure of proteins from UV circular dichroism spectra using an unsupervised learning neural network. *Protein Eng. 6*, 383−390.
(53) Unneberg, P., Merelo, J. J., Chacon, P., and Moran, F. (2001) SOMCD: Method for evaluating protein secondary structure from UV circular dichroism spectra. *Proteins 42*, 460−470.
(54) Chen, Y. H., Yang, J. T., and Martinez, H. M. (1972) Determination of the secondary structures of proteins by circular dichroism and optical rotatory dispersion. *Biochemistry 11*, 4120−4131.
(55) Qin, Z., Kalinowski, A., Dahl, K. N., and Buehler, M. J. (2011) Structure and stability of the lamin A tail domain and HGPS mutant. *J. Struct. Biol. 175*, 425−433.
(56) Kapinos, L. E., Burkhard, P., Herrmann, H., Aebi, U., and Strelkov, S. V. (2011) Simultaneous formation of right- and left-

handed anti-parallel coiled-coil interfaces by a coil2 fragment of human lamin A. *J. Mol. Biol. 408*, 135−146.
(57) Taimen, P., Pfleghaar, K., Shimi, T., Moller, D., Ben-Harush, K., Erdos, M. R., Adam, S. A., Herrmann, H., Medalia, O., Collins, F. S., Goldman, A. E., and Goldman, R. D. (2009) A progeria mutation reveals functions for lamin A in nuclear assembly, architecture, and chromosome organization. *Proc. Natl. Acad. Sci. U.S.A. 106*, 20788−20793.
(58) Lupas, A. N., and Gruber, M. (2005) The structure of α-helical coiled coils. *Adv. Protein Chem. 70*, 37−78.
(59) Zhou, N. E., Kay, C. M., and Hodges, R. S. (1992) Synthetic model proteins. Positional effects of interchain hydrophobic interactions on stability of two-stranded α-helical coiled-coils. *J. Biol. Chem. 267*, 2664−2670.
(60) Meier, M., Stetefeld, J., and Burkhard, P. (2010) The many types of interhelical ionic interactions in coiled coils: An overview. *J. Struct. Biol. 170*, 192−201.
(61) Strelkov, S. V., and Burkhard, P. (2002) Analysis of α-helical coiled coils with the program TWISTER reveals a structural mechanism for stutter compensation. *J. Struct. Biol. 137*, 54−64.
(62) Strelkov, S. V., Herrmann, H., Geisler, N., Wedig, T., Zimbelmann, R., Aebi, U., and Burkhard, P. (2002) Conserved segments 1A and 2B of the intermediate filament dimer: Their atomic structures and role in filament assembly. *EMBO J. 21*, 1255−1266.
(63) Cohen, C., and Parry, D. A. D. (1986) α-Helical coiled coils: A widespread motif in proteins. *Trends Biochem. Sci. 11*, 245−248.
(64) Cohen, C., and Parry, D. A. (1990) α-Helical coiled coils and bundles: How to design an α-helical protein. *Proteins 7*, 1−15.
(65) Lupas, A. (1996) Prediction and analysis of coiled-coil structures. *Methods Enzymol. 266*, 513−525.
(66) Lupas, A., Van Dyke, M., and Stock, J. (1991) Predicting coiled coils from protein sequences. *Science 252*, 1162−1164.
(67) Zwerger, M., Jaalouk, D. E., Lombardi, M. L., Isermann, P., Mauermann, M., Dialynas, G., Herrmann, H., Wallrath, L. L., and Lammerding, J. (2013) Myopathic lamin mutations impair nuclear stability in cells and tissue and disrupt nucleo-cytoskeletal coupling. *Hum. Mol. Genet.*, DOI: 10.1093/hmg/ddt079.
(68) Pasotti, M., Klersy, C., Pilotto, A., Marziliano, N., Rapezzi, C., Serio, A., Mannarino, S., Gambarin, F., Favalli, V., Grasso, M., Agozzino, M., Campana, C., Gavazzi, A., Febo, O., Marini, M., Landolina, M., Mortara, A., Piccolo, G., Vigano, M., Tavazzi, L., and Arbustini, E. (2008) Long-term outcome and risk stratification in dilated cardiolaminopathies. *J. Am. Coll. Cardiol. 52*, 1250−1260.